Geotextiles and Geomembranes 53 (2025) 681–696

Contents lists available at ScienceDirect

Geotextiles and Geomembranes

journal homepage: www.elsevier.com/locate/geotexmem

Regular Paper

Experimental study on the vacuum consolidation of recycled fibre-improved soft soils assisted with prefabricated vertical drain☆

Kai Lou [a,b], Zhen-Yu Yin [b,*], Ding-Bao Song [b], Wei-Feng Huang [b]

[a] College of Civil and Transportation Engineering, Shenzhen University, Shenzhen, China
[b] Department of Civil and Environmental Engineering, The Hong Kong Polytechnic University, Hong Kong, China

ARTICLE INFO

Keywords:
Soft soil
Consolidation
Vacuum preloading
Wasted face mask fibre
Biodegradable prefabricated vertical drain

ABSTRACT

Billions of face masks were discarded daily, causing severe environmental concerns. Recycling waste face masks presents a significant challenge. Meanwhile, the traditional vacuum preloading shows limitations on the performance on soft soil ground. This paper investigates the potential benefits of reusing Face-Mask Fibres (FMF) as an admixture to enhance the treatment effects of vacuum preloading on soft soils. The performance of an environmentally biodegradable type of Prefabricated Vertical Drain (PVD) is also compared with that of conventional PVD through a series of laboratory physical model tests. The settlement, distributions of vacuum pressure, porewater pressure, and water content were monitored. In addition, after vacuum preloading, the undrained shear strength of treated soil was determined. Scanning electron microscope tests were also carried out to analyse the microscopic structure of treated soil. Results reveal that face-mask fibres significantly improved the performances of vacuum preloading in terms of vacuum dewatering and strengthening. Furthermore, the rate of vacuum consolidation was accelerated due to the additional drainage channels provided by recycled face-mask fibres. Notably, the final water content of the treated soil decreased to 41.8%, which is markedly lower than the liquid limit of 63.9%. The undrained shear strength exhibited considerable improvement, nearly doubling in value. The mechanism of how FMF works was also discussed.

1. Introduction

The global outbreak of the novel coronavirus COVID-19 hit the world. It has had a profound impact on the daily lives of people worldwide. One of the most significant changes brought about by the pandemic is the massive use of face masks, which have become an essential daily item. It is estimated that 129 billion face masks were discarded monthly during the early stage of the pandemic Wang et al. (2023a). The disposal of billions of face masks has emerged as a critical issue. Melt-blown nonwoven fabric is the major material for making quality face masks. The melt-blown nonwovens are made of thermoplastic synthetic polymer, directly from the polymer stage to randomly-laid nonwoven fabrics by the melt-blown spinning process. The melt-blown web has a smaller pore size with greater filtration efficiency in comparison with spun-bonded fibrous webs. Because of its lesser strength, in most filter applications, this melt-blown fibrous media is used with support from another web or as part of a composite structure. The most widely used polymer for this web formation is polypropylene (PP). Given their chemical composition, the disposal of used face masks presents a significant environmental challenge. As such, the proper management of face mask waste has become a pressing issue, requiring innovative solutions to mitigate their environmental impact. Finding sustainable and efficient ways to recycle this waste is crucial for mitigating the environmental impact of the pandemic and ensuring the continued health and safety of communities worldwide.

In response, there has been growing interest in exploring innovative and sustainable approaches to address the issue (Tang et al., 2021). The utilization of sterilized waste materials in construction engineering has emerged as a promising and viable solution. This not only helps to reduce the volume of waste sent to landfills but also provides a valuable resource for geotechnical engineering projects. Recently, scholars attempted to use face masks as an admixture to enhance the engineering properties of concrete and granular soils, and the results revealed that the beneficial reuses are appreciable (Barforoush et al., 2024;

☆ Manuscript prepared for the submission of Geotextiles and Geomembranes

* Corresponding author.
E-mail addresses: kailou@szu.edu.cn, kai.lou@connect.polyu.hk (K. Lou), zhenyu.yin@polyu.edu.hk (Z.-Y. Yin), dingbao.song@polyu.edu.hk, dingbao_song@126.com (D.-B. Song), weifeng-henry.huang@connect.polyu.hk (W.-F. Huang).

https://doi.org/10.1016/j.geotexmem.2025.01.002
Received 9 September 2024; Received in revised form 11 January 2025; Accepted 12 January 2025
Available online 20 January 2025

Table 1
Basic properties of Hong Kong marine deposit.

Property	Value
Natural water content (%)	86.3
Liquid limit (%)	63.9
Plastic limit (%)	28.2
Plasticity index	35.7
Specific gravity	2.63
Salinity (%)	3.3

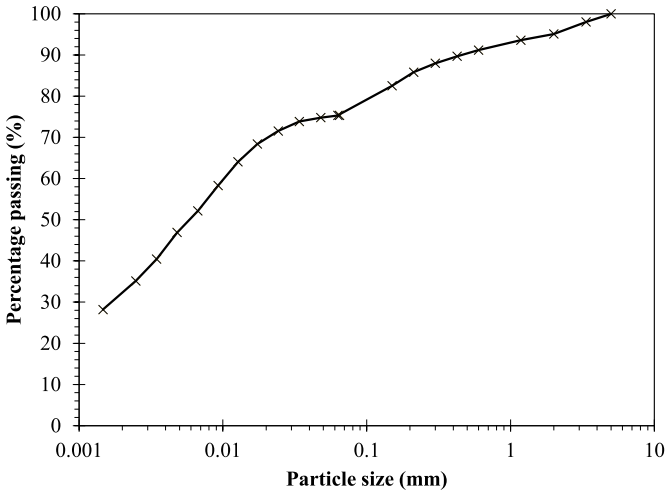

Fig. 1. Particle size distribution of Hong Kong marine deposits.

Kilmartin-Lynch et al., 2021; Saberian et al., 2021). However, studies on using waste face masks on clayey soils still lack (Rehman and Khalid, 2021; Wang et al., 2023b).

On the other hand, the common Prefabricated vertical drain (PVD) comprises polymers, which is hardly degraded, causing environmental concerns. PVD assisted by surcharge or vacuum preloading has been widely used to improve soft soil ground because of its simple construction procedure and remarkable effects (Chu et al., 2012). Since Kjellman (1948) first proposed the so-called cardboard wick, the prototype of prefabricated drains, PVD has been widely adopted in ground improvement in recent decades. Similar to the sand drain, PVD can significantly shorten the drainage path of the soft soil layer and accelerate the consolidation process as a result. The prefabricated drain is vertically inserted into the soil layers. Usually, the permeability in the horizontal direction is higher than the vertical one so that the porewater can first move horizontally toward the PVD and then be discharged via the PVD. The consolidation is thus further accelerated. The improvement effect of PVD has been widely studied (Chu et al., 2009; Fang and Yin, 2006; Hansbo, 1960, 1979; Hansbo et al., 1981; Ngo et al., 2020; Nguyen et al., 2015; Wang et al., 2018). PVD initially works with surcharge preloading, while vacuum preloading has been preferred in recent years because of the maturity of sealing technology (Chai et al., 2006, 2010; Chai and Carter, 2013; Dong, 2018; Kumarage and Gnanendran, 2019; Lam et al., 2020; Long et al., 2015; Wu et al., 2022). Vacuum preloading is commonly incorporated with a sand cushion, and engineers developed a so-called Beaudrain system that directly connects the PVDs to the vacuum pump by a horizontal tube to replace the sand layer (Bergado et al., 2008; Corlever et al., 2006). Recently researchers made improvements on the PVD joint to simplify the construction process further (Lam et al., 2020; Long et al., 2015; Wang et al., 2016, 2018). Continuing to enhance the efficiency of this method remains a primary goal for scholars. Zhou et al. (2022) reviewed various improvements to the conventional vacuum preloading technique, which involve methods such as replacing or eliminating one or more components of the vacuum preloading system and integrating it with other soil improvement techniques. Nowadays, PVD is a proven technique, but concerns still exist. After vacuum preloading, the water content decreases to around the liquid limit, which is still too soft for subsequent constructions. In other words, traditional vacuum preloading can only work as a preliminary treatment, and further treatment is still required.

Besides, the traditional PVD comprises polymers, such as polyethene and polypropylene, that cannot be degraded after completing their drainage function (Jewell, 1996; Nguyen and Indraratna, 2023). The PVD will be left in the ground and cannot be naturally degraded, interfering with the subsequent construction of piles or foundations, if any. Therefore, scholars are interested in biodegradable prefabricated drains made from natural materials (Lee et al., 1994). Particularly, the agricultural waste is preferred as a way to sustainable waste management. Jeon et al. (2003) attempts to make a PVD using waste cotton fibres as the filter material and aliphatic polyester-based plastic as cores, both of which are biodegradable. Nguyen and Indraratna (2017a) and Nguyen and Indraratna (2017b) investigate the hydraulic behaviour of coir fibre drains in experimental aspect and provide numerical frameworks for prediction. Nguyen et al. (2018, 2020) further studied the performance of a biodegradable PVD made from coconut cores wrapped in Indian jute sheath filters. Researchers proposed and validated the possibility of using crop stalks as the raw material for making the PVD core (Kaewthai and Chooglin, 2015). Crop stalks are the agricultural waste after the harvest of crops such as corn and wheat, which are fully organic and naturally degradable. Yuan et al. (2024) investigates the degradation of straw-based wick drains and its effect on consolidation. It will be more environmentally friendly if the biodegradable PVD can be widely adopted in future constructions. Even the degradation time of the new PVD can be adjusted in the production to meet the requirements of different construction.

Overall, the utilization of biodegradable PVDs and waste face masks provides a way for sustainable waste management and advancements in geotechnical engineering. Therefore, to improve the treatment efficiency of the existing vacuum preloading method, this paper proposes an eco-friendly soil improvement method using face mask fibre (FMF) as an admixture to the soil and the biodegradable PVD incorporated with the vacuum preloading technique. A series of laboratory physical model tests on soft soil slurry is conducted to compare the performance of different PVDs and examine the applicability of the proposed eco-friendly treatment method. The settlement, water content, porewater pressure, and the mass of water discharged by vacuum are monitored during the vacuum consolidation. After vacuum preloading, the shear strength of treated soils is examined. Meanwhile, the microstructure of treated soils is analysed through the scanning electron microscope (SEM) technique.

2. Experimental methodology

2.1. Soils used in model tests

Hong Kong is one of the most developed regions in the world and continues to experience rapid development. Hong Kong Marine Deposits (HKMD) is a common and typical soil on the neighbouring seabed. The study on HKMD holds the potential to benefit practical engineering applications in this region and the nearby Great Bay Area of South China. Therefore, a mud-like sample dredged from a construction site in Tuen Mun, Hong Kong, was used in the tests. Basic properties of the tested soil, listed in Table 1, were determined according to the British standard BS1377:2016 (British Standards Institution, 2016). The natural mud is in a fluid state as the natural water content, 86.3%, is approximately 1.35 times the liquid limit. The particle size distribution (PSD) curve (Fig. 1) shows that the natural Hong Kong marine deposit is composed of clay (28.4%), silt (48.1%) and sand (23.5%). According to the result of the XRD test, the major minerals of HKMD are Kaolinite,

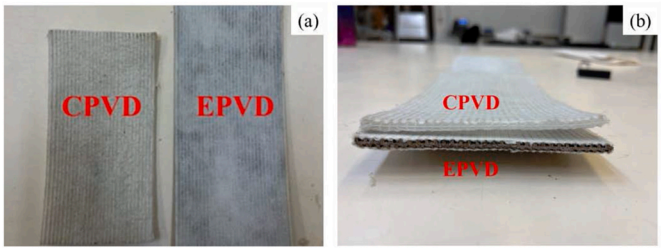

Fig. 2. Section views of CPVD and EPVD: (a) Filter; (b) Core.

Table 2
Properties of CPVD and EPVD.

	Index (Unit)	CPVD	EPVD	Note
Integrated body	Thickness (mm)	5	5.5	/
	Width (mm)	100	99.6	/
	Failure tensile strength (kN/10 cm)	≥3.5	3.95	Elongation 10%
	Vertical drainage (ml/s)	≥50	52.6	Under 350 kPa lateral pressure
Filter	Tensile strength (dry state)	≥25	22.5	/
	Tensile strength (wet state)	≥20	10.5	/
	Permeability coefficient (cm/s)	$\geq 5*10^{-3}$	$1.5*10^{-2}$	Water soaking 24 h
	Filter apparent opening size (μm)	120	74	According to O_{95}, adjustable

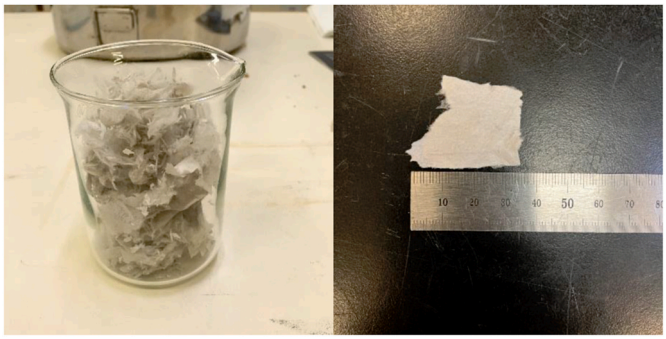

Fig. 3. Shredded face masks used in the study.

Mica, and Quartz, which correspond to clay, silt, and sand, respectively. Based on the Casagrande plasticity chart, this soil can be categorised as fat clay with sand according to the ASTM standard (ASTM, 2017). Since the soil on the plasticity chart is very close to the A-line, it may exhibit the characteristics of both silt and clay.

2.2. PVD and face mask

Two types of PVD were used in this study. One is the Conventional PVD (CPVD) commonly used in construction, and the other is the new Eco-friendly PVD (EPVD) that is mainly made up of compressed crop stalks. Fig. 2 shows the appearance of the two PVDs. Both PVDs are integrated types. The filter is attached to the core via heat-melting to form an integrated body, which increases its tensile strength and discharge capacity compared to the traditional PVD (Cai et al., 2017; Liu and Chu, 2009). Filters of both PVDs are nonwoven fabric. The main difference between the two PVDs is the core. The core of CPVD is comprised of polyethene (PE) and polypropylene (PP), which presents a white colour as Fig. 2 shows. Meanwhile, the core of EPVD is compressed crop stalk, which shows a dark colour and is the agricultural waste after the harvest of crops. This material is fully organic and naturally degradable. The crop stalk is compressed into a plate with a harmonica shape, the same as the CPVD. This plate serves as the core of EPVD. Both types of prefabricated drains meet the ASTM standard requirement (ASTM, 2022). The vertical drainage performance is assessed on the PVD covered with a latex membrane under 350 kPa lateral pressure and a hydraulic gradient of 0.5. The failure tensile strength is measured at a tensile strain rate of 50 mm/min with an elongation of 10%. The permeability coefficient is determined using a filter with an area greater than 20 cm^2 under a constant water head. The typical properties of the two types of PVD are presented in Table 2.

The face mask used in this study is the three-layer surgical mask, the most common type of face mask in daily use. Considering the hygiene, all face masks used in this series of tests were brand new and unused. In a real application, used face masks must be properly sterilized by several steps such as alcohol and ultraviolet disinfection, and high temperature sterilization. The masks in this research are shredded into small pieces using a commercial textile shredder. The shape and size of face mask pieces are random after the shredding. Some of the shredded pieces are too big for this test, considering the size of the physical model. In order to ensure the homogeneity of tested materials, large face mask pieces are further processed and only those with dimensions smaller than 3 cm × 3 cm are used in the tests (Fig. 3).

2.3. Experimental apparatus

The experimental apparatus, self-developed for this study, mainly consists of a cylindrical tank and vacuum loading system. Fig. 4 shows the schematic and photo of the test system.

The cylindrical tank consists of several short acrylic tubes called sub-columns. Each sub-column is 100 mm in height and 170 mm in internal diameter. The thickness of the wall of the acrylic tube is 10 mm to ensure safety when loading. Eight sub-columns were used and assembled to have an 800 mm initial height for each test in this study. The diameter of the tank might seem too small to represent a representative cell of the periodic pattern of the prefabricated drains (generally square- or triangle-patterned) when considering the common PVD spacing in real engineering. However, this study focuses on the improvement effects of FMF on vacuum preloading. Given the extensive study of conventional vacuum preloading by PVD alone over decades, the radial characteristics of vacuum preloading are deemed unnecessary for this research. Focusing on one-dimensional consolidation characteristics of the soils under vacuum load would be more efficient in terms of test duration and workload. Particularly, a smaller size could significantly reduce the test period. Therefore, this size was chosen.

There are three holes opened at the middle height of each sub-column. Two of them serve as sampling ports with valves. Soils can be extracted from sampling ports at different heights during tests so that the variation of the water content profile can be obtained. Meanwhile, other holes on the sidewall are pressure ports for porewater pressure monitoring via pressure transducers. Scales are stuck on the internal wall of the column to avoid the refraction influence of acrylic on the scale reading. The settlement of the soil surface during self-weight consolidation can be recorded by digital cameras reading the scales on the sidewall due to the transparent feature of the acrylic material. The positions of digital cameras should be frequently adjusted to the soil height to ensure the accuracy of scale reading. LVDT is used for settlement monitoring after PVD installation.

The vacuum system consists of a vacuum pump and a water-gas separator. The vacuum pump, water-gas separator and PVD are connected in sequence through pipes. The water-gas separator is used to separate air and the water discharged by vacuum pressure. It is put on an electronic balance to monitor the mass of the discharged water.

All transducers have been calibrated, and the tightness of the apparatus only filled with water has been carefully examined before each test.

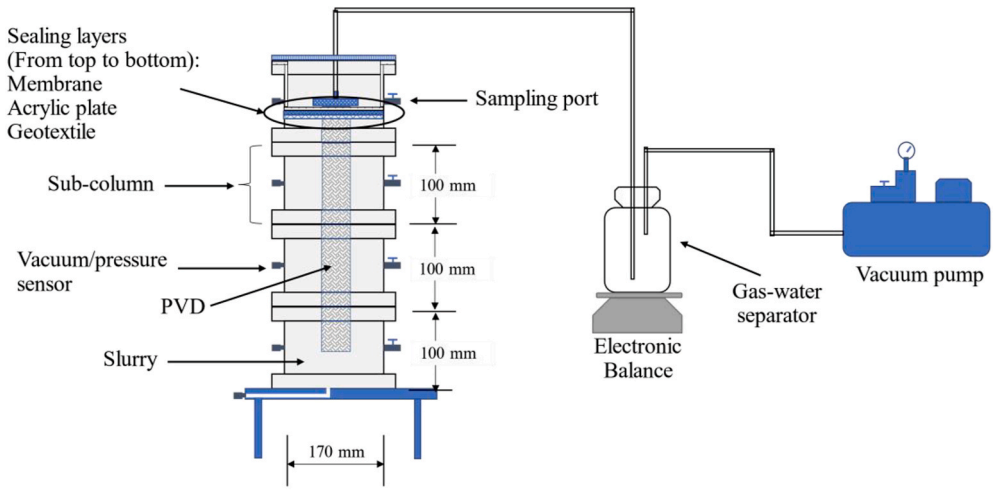

(a) Schematic of the test system

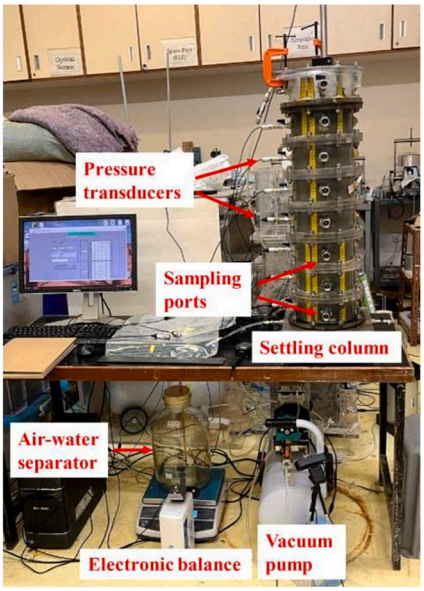

(b) appearance of the test system

Fig. 4. Apparatus of physical model tests.

2.4. Experimental procedure

First, the slurry-state HKMD was poured into the settling column to a height of 800 mm. The initial water contents of the HKMD before pumping into the model of the three tests are 202.2%, 204.4% and 203.3%, respectively. The sedimentation process would be completed quickly. After that, the soil slowly consolidated under its self-weight before loading. The soil can be considered stable in the self-weight consolidation stage. Therefore, to eliminate the influence of the initial conditions, the slurry was first left standing for 4 days for sedimentation and self-weight consolidation without any treatment to reach a stable state before applying the vacuum load for each test. Then the main stage begins.

The PVD was inserted into the soil column centre along with two steel plates. The steel plates served as the mandrel in construction practice to ensure that the installed PVD was vertical in the ground and were pulled out after the PVD installation (Fig. 5). The top end of the PVD was linked to a flexible tube via a customised T-shaped connector (Fig. 6a). The tube was connected to the water-gas separator and vacuum pump in turn so that the vacuum pressure could be applied to the soil via the PVD. From bottom to top, a layer of a geotextile, a light acrylic plate and a layer of geomembrane were laid on the soil surface (Fig. 6b). The geotextile was to avoid soil loss from the connecting point between the T-connector and the sealing layer. The acrylic plate was to ensure an even soil surface, and the geomembrane sealed the model. In this stage, an LVDT was placed on the outside top of the geomembrane to monitor the settlement. Finally, the vacuum load started gradually.

Note that the height after self-weight consolidation slightly varied in the three tests. The PVD length should be slightly smaller than the soil height to avoid the PVD bending at the very beginning. Therefore, the size of PVDs used in this series of tests is 650 mm in length and 35 mm in width. As the full width of a PVD is 100 mm, the PVDs were cut to fit the dimension and the side edges were sealed using adhesive to avoid the loss of soil particles via the side channels.

The surface settlement, mass of discharged water, porewater pressure and vacuum pressure were closely monitored during tests. Soil samples were extracted from the model through sampling ports during tests. Note that sampling was more frequent at the early stage after starting the vacuum loading. In general, soil samples were taken at 2 h, 8 h, 1 d, 2 d, 4 d, 8 d, 16 d and the end of vacuum preloading. Finally,

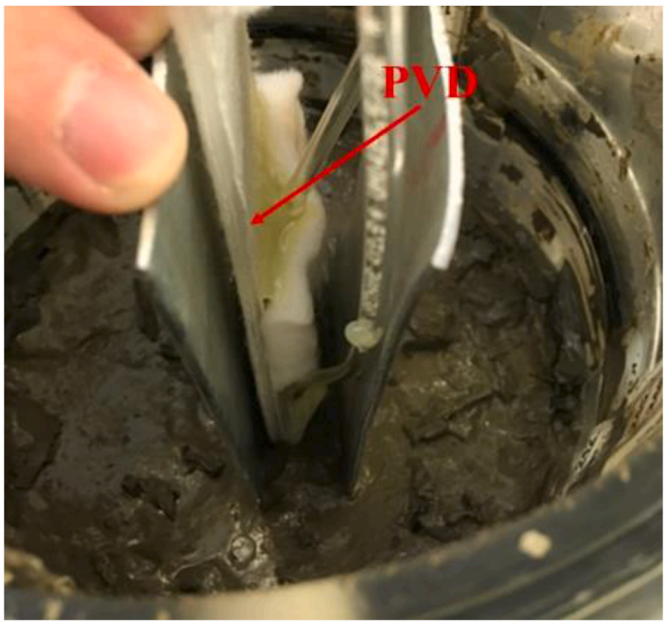

Fig. 5. PVD installation.

these tests were terminated once the settlement or the porewater pressure dissipation became stable.

2.5. Test program

Three physical model tests were carried out: namely, Test 1, Test 2, and Test 3. Test 1 and Test 2 used CPVD and EPVD, respectively. Test 3 considered the effects of FMF. Test program is summarized in Table 3. Based on the results of a series of element tests on HKMD, which is discussed in another paper, the optimal mixing ratio of face mask fibre to soil is 0.5% in mass, within a feasible fibre content from 0% to 1%. Particularly, the permeability is significantly improved at this ratio (see Fig. 7). As the FMF content rises from 0 to 0.5%, the permeability coefficient escalates from less than 0.4×10^{-9} m/s to approximately 3×10^{-9} m/s, which is an increase of nearly one order of magnitude. This paper does not focus on providing an optimal mixing ratio but a comprehensive treatment technique using eco-friendly materials. Therefore, in Test 3, face mask fibres were mixed into the HKMD slurry with a mass proportion of 0.5%, and EPVD was used in this test.

The three tests followed the same multi-staged vacuum loading path, and Fig. 8 shows the loading stages and durations. Wang et al. (2021) highlighted that reducing the vacuum gradient could mitigate the migration of fine particles to the prefabricated drains, thereby reducing the differential settlement of the soil surface. Therefore, the small vacuum gradient leads to decreased clogging of the PVD and promotes uniform soil consolidation. Particularly, Wang et al. (2021) found that the vacuum gradient of 20 kPa reaches a balance between the

Table 3
Test program.

No.	PVD type	Adding FMF
Test 1	CPVD	No
Test 2	EPVD	No
Test 3	EPVD	Yes

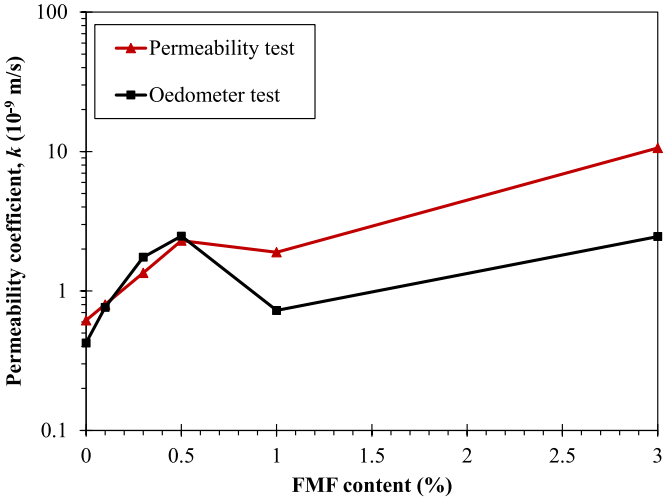

Fig. 7. Relationship between permeability coefficient and FMF content.

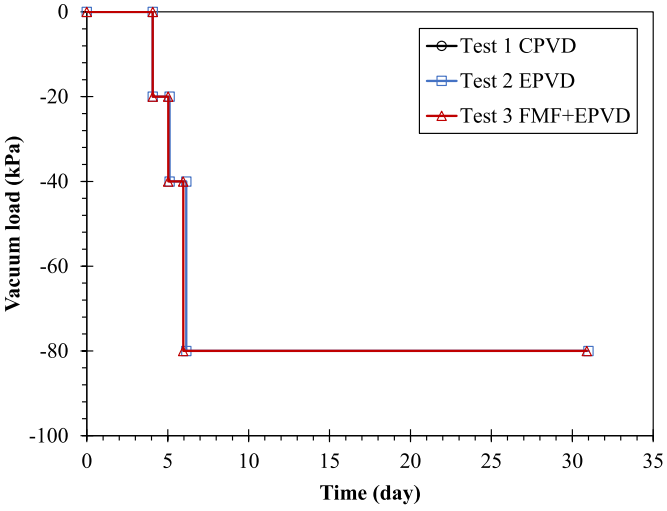

Fig. 8. Schedule for the application of vacuum pressures.

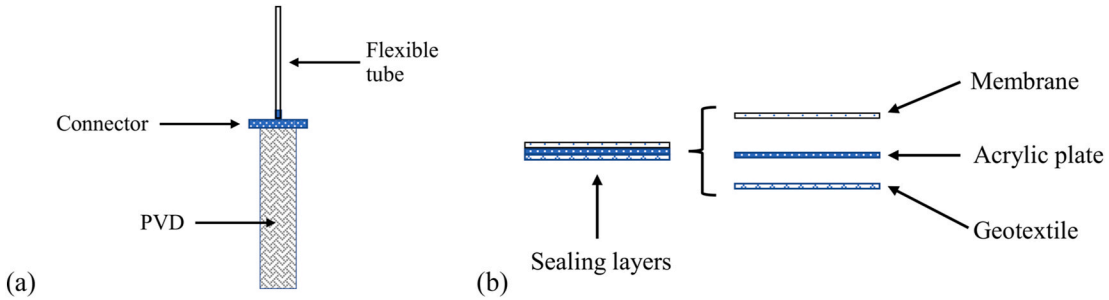

Fig. 6. Detailed schematic of PVD system: (a) PVD and T-connector; (b) sealing layers.

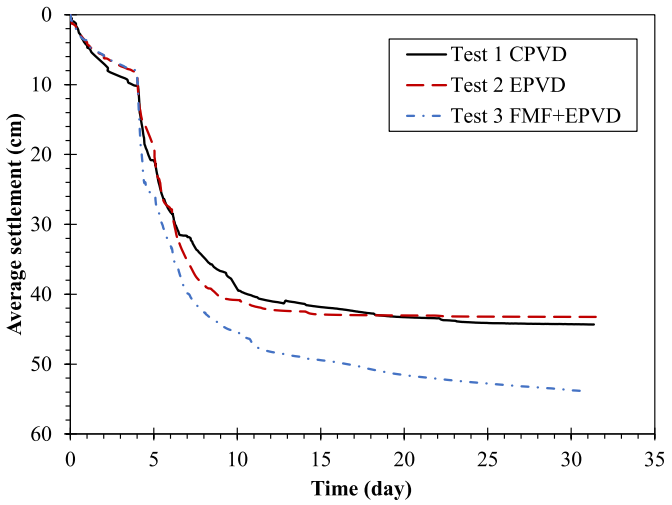

Fig. 9. Comparison of surface settlements of the three tests.

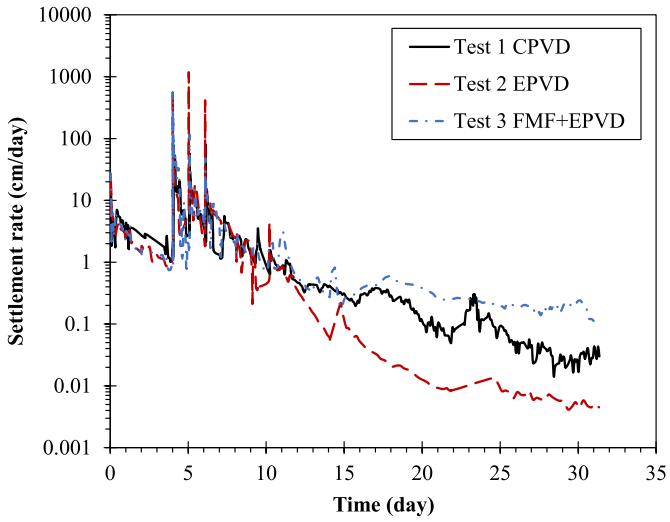

Fig. 11. Comparison of settlement rate of the three tests.

Table 4
Heights of the soil surface and final strains.

Test No.	Height before loading, h_1 (cm)	Final height, h_f (cm)	Settlement (cm)	Final strain, ε_f (%)
Test 1 CPVD	68.69	34.58	34.11	49.65
Test 2 EPVD	70.06	35.29	34.77	49.63
Test 3 FMF + EPVD	69.98	24.61	45.37	64.83

Note: The final height and final strain correspond to the state at the end of each test, although the settlement kept increasing at the end of Test 3.

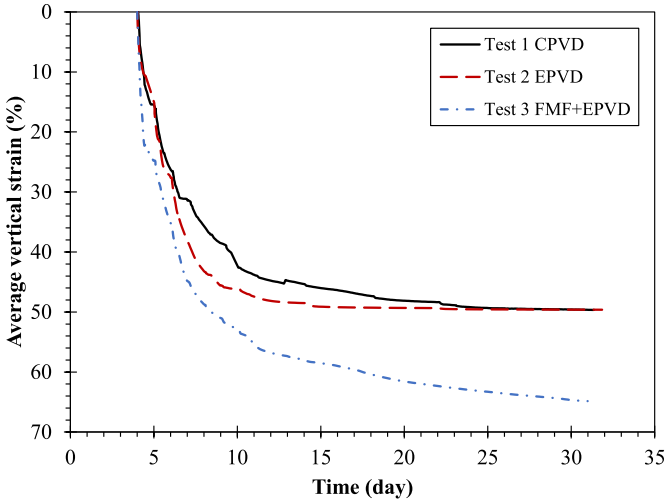

Fig. 10. Comparison of vacuum consolidation strain of the three tests.

clogging-alleviating effect and the required vacuum duration. This paper adopted the loading procedure as suggested by Wang et al. (2021) to eliminate the clogging effect around the prefabricated drain. The marine deposit slurry in the column tank first settled and consolidated under its self-weight for 4 days. After that, vacuum pressures of −20 kPa and −40 kPa were maintained for 1 day only, and the final −80 kPa load remained till the end of the test. The consolidation characteristics and performances of two PVDs and FMF under vacuum load can thus be compared and evaluated via this series of tests.

After vacuum preloading, final water contents and undrained shear strengths were measured. Scanning electron micrographs of the treated soils, FMF and PVD filters were analysed.

3. Results and discussions

3.1. Settlement and vertical strain

The settlements of the three tests are plotted in Fig. 9. Final settlements of Test 1, Test 2 and Test 3 are 44.32 cm, 43.28 cm, and 53.85 cm, respectively. The result clearly shows that the soil mixed with FMF reaches the largest settlement. However, because of the heterogeneity of natural HKMD, the heights of these tests before loading are slightly different. The settlement that occurred during the vacuum consolidation was normalised into engineering strain to conveniently compare the deformation of these tests. The heights before and after applying vacuum pressure, i.e. h_1 and h_f, and corresponding final strains (ε_f) are listed in Table 4. The final strain denoting the deformation under vacuum load is calculated based on the following equation.

$$\varepsilon_f = \frac{h_1 - h_f}{h_1} \tag{1}$$

Strain variations are shown in Fig. 10. Final strains of the three tests are 49.65%, 49.63%, and 64.83%, respectively. The final strains of CPVD and EPVD cases (i.e., Test 1 and Test 2) are almost the same, indicating that the two types of PVD generally have no significant difference in performance. The soil mixed with FMF (i.e. Test 3) reaches the largest deformation (64.83%), which is about 15% higher than the other two tests without FMF. Since the two PVDs function similarly, the significant increase in deformation in Test 3 can be attributed to the FMF, marking the effectiveness of FMF in enhancing the consolidation.

To directly compare the rate of settlement, the settling rate ($\dot{s}$) is defined by the ratio of settlement change to the corresponding time interval using 10 adjacent data points.

$$\dot{s} = \frac{s_{i+5} - s_{i-5}}{t_{i+5} - t_{i-5}} \tag{2}$$

Regarding the settling rate (see Fig. 11), the curves of Test 1 and Test 2 show that the EPVD facilitates consolidation more rapidly than CPVD in the initial stages. However, the settling rate in the EPVD test also decreases earlier, dropping below 0.1 cm/day after Day 15. The properties of the two PVDs may be attributed to the difference in the early settling rate. The EPVD is 0.5 mm thicker than the CPVD, and the permeability coefficient of the EPVD filter is also greater. Hence the drainage capacity of EPVD surpasses that of CPVD. Especially at the early stage, the consolidation is significant and the PVDs work fully with

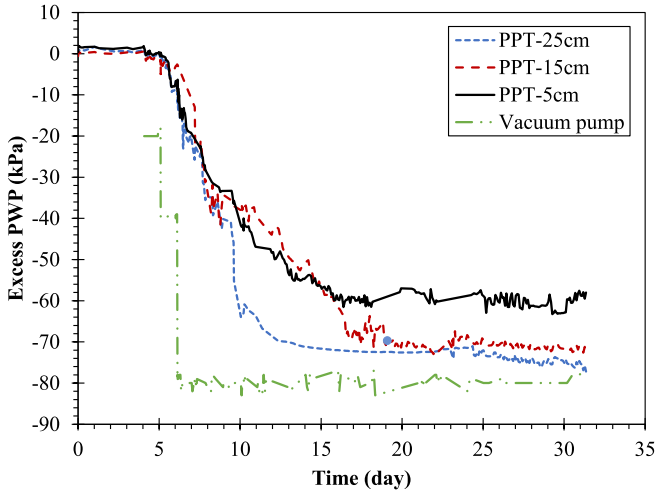

(a) Test 1 CPVD

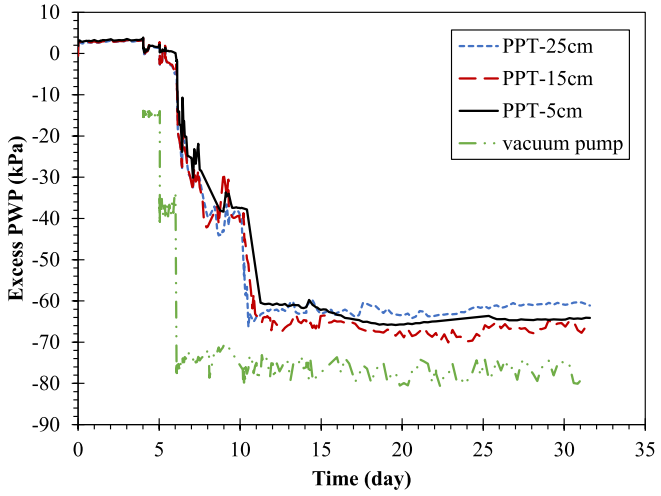

(b) Test 2 EPVD

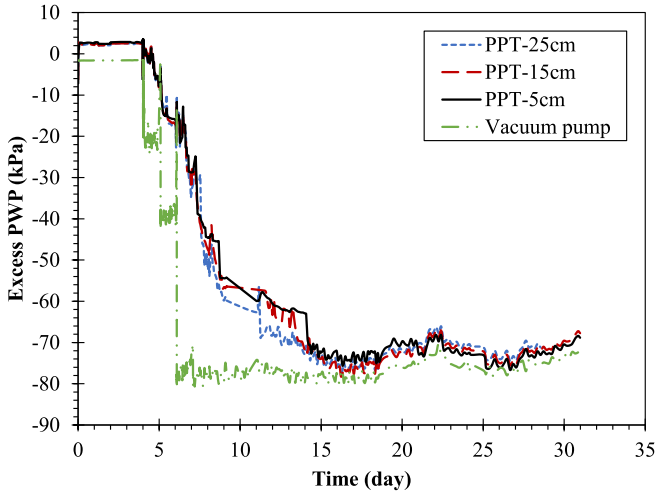

(c) Test 3 FMF+EPVD

Fig. 12. Variation of excess porewater pressures during consolidation.

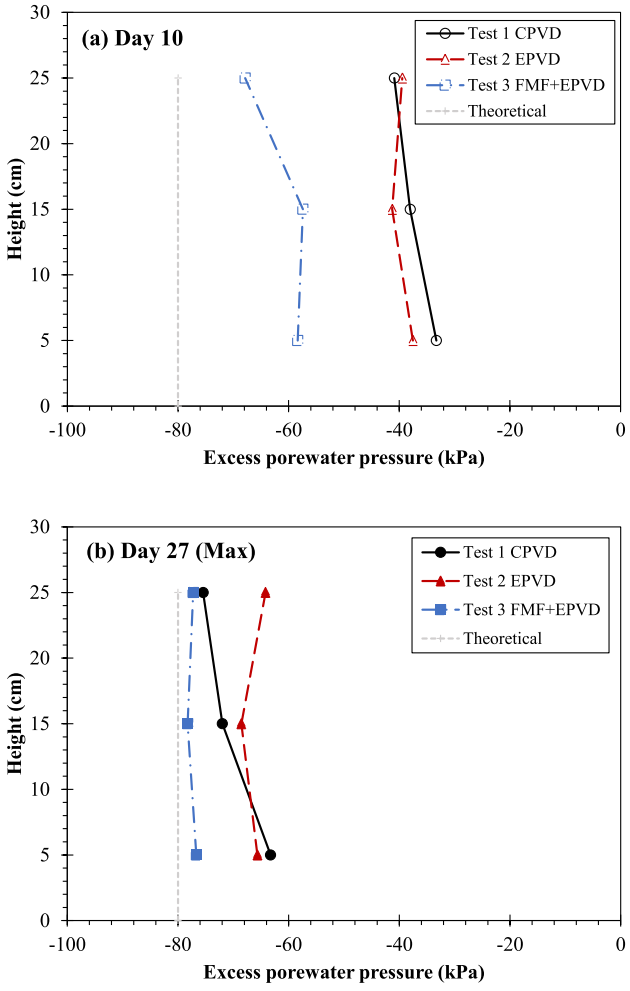

Fig. 13. Distribution of excess porewater pressure: (a) Day 10 and (b) Day 27.

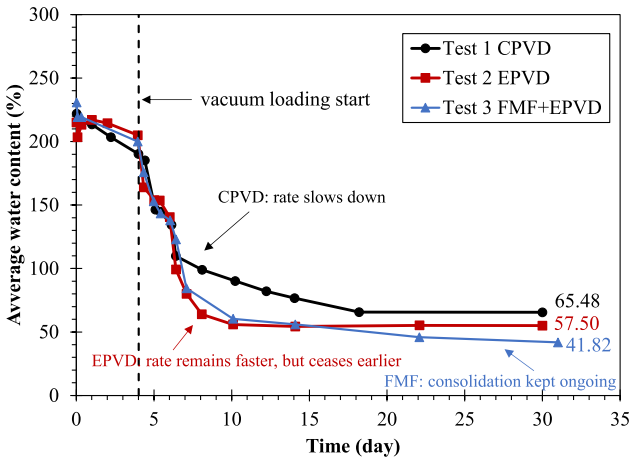

Fig. 14. Comparison of average water content variation.

their capacities. Fig. 11 shows that the maximum settlement rate of Test 1 is around 100 cm/day, while that of Test 2 and Test 3 using EPVD reaches 1000 cm/day. Later, PVDs bent as the settlement increased, diminishing their abilities and leading to a decrease in the settlement rate. Meanwhile, the soil became dense, hindering the porewater movement within the soil. From now on, it is the dense zone of the soil

Table 5
Average water content.

Test No.	Water content before loading, w_1 (%)	Final water content, w_f (%)	Absolute decrease (%)	Percentage decrease, R_w (%)
Test 1	190.14	65.48	124.66	65.6
Test 2	204.97	57.50	147.47	71.9
Test 3	198.30	41.82	156.48	78.9

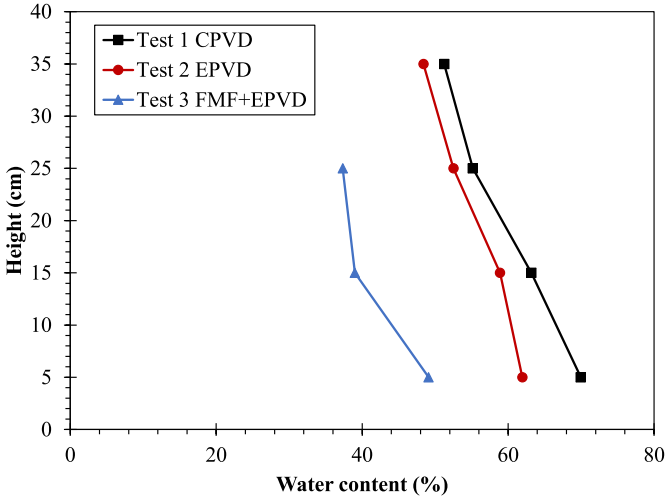

Fig. 15. Average water content profiles after vacuum consolidation test.

surrounding the PVD that determines the rate instead of the PVD drainage capacity.

However, the result of Test 3 shows apparent differences. The soil settled faster during the whole process and reached a larger settlement, compared to the other tests. The settlement rate remained higher than 0.1 cm/day, indicating that FMF works. FMF provided additional drainage channels within the soil so that the porewater could be dissipated more and faster, resulting in a faster and larger settlement. Particularly, its influence became significant after the PVD experienced severe bending. Comparing the two tests using EPVD (i.e. Test 2 and Test 3), the FMF-treated soil yields a 15.15% higher strain than the natural HKMD at the test end, which is a considerable improvement.

It can be noticed that the settlement rate is similar among the three tests at the very beginning (i.e. around first 5 days). The FMF-improved soil shows no significant effects. The reason could be that the soil structure is not formed yet during the initial phase. Deformation mainly involves the free settling of soil particles in the fluid, rather than the general consolidation. Water and soil particles can move without much hindrance. However, following the application of vacuum load, a relatively dense soil structure gradually forms. Deformation transitions to consolidation, involving the dissipation of pore water from the soil structure through compression. At that time, the dissipation of pore water is limited by the soil structure's permeability. Particularly, soils compact intensively under vacuum pressure, leading to reduced permeability with settlement, thereby decelerating consolidation. Pore water hardly moves through the soil structure. Consequently, settlement is impeded in tests without FMF.

In contrast, the addition of FMF provides additional channels for water dissipation. The consolidation is thus faster in the soil with the assistance of FMF, especially in later stages. The mechanism of how FMF enhances permeability will be discussed in the later Microstructure Analysis section.

FMF is a softer material than the soil structure, resulting in a higher compressibility of FMF-treated soil under the same stress conditions compared to the natural HKMD, which may also affect the settlement.

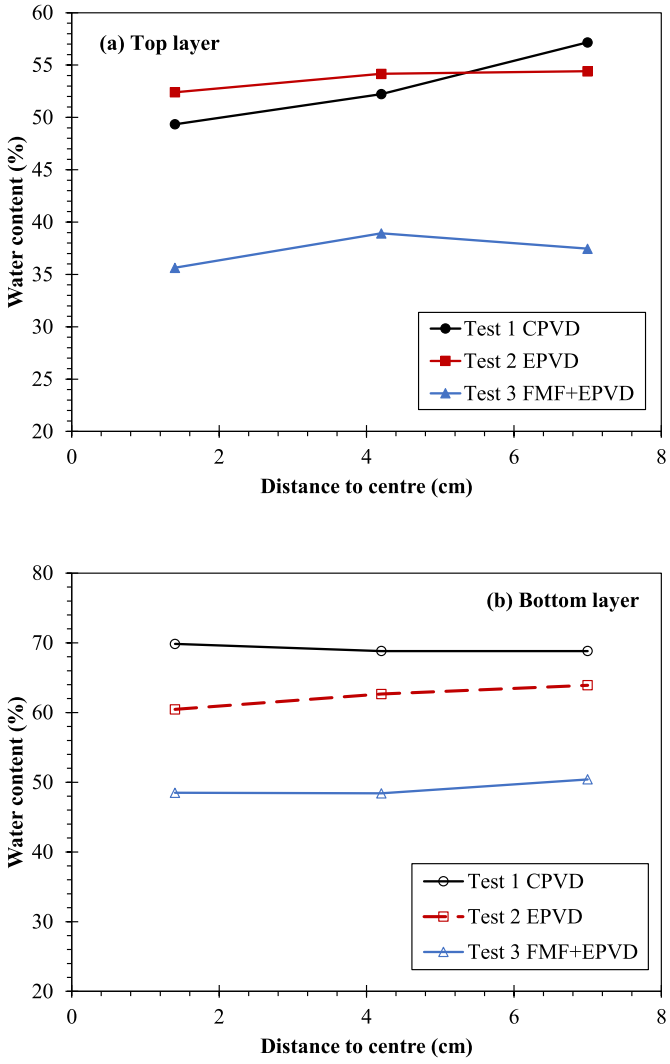

Fig. 16. Radial water content profile after vacuum preloading: (a) Top layer and (b) Bottom layer.

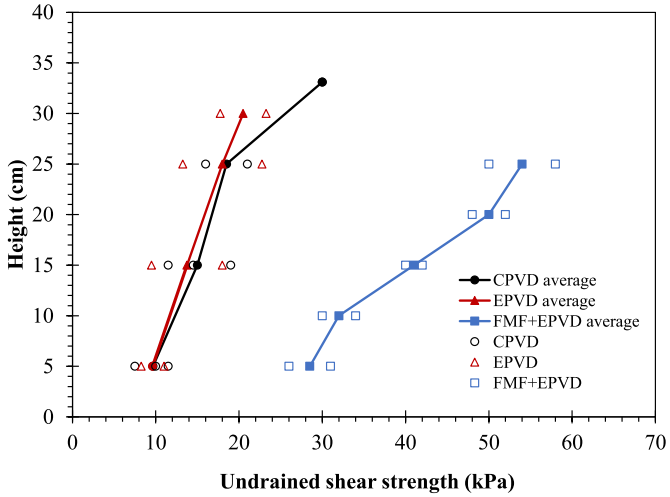

Fig. 17. Vane undrained shear strength profile measured at test end.

The compression indexes (C_c) of natural HKMD and FMF-treated HKMD with a mass mixing ratio of 0.5% obtained from oedometer tests are 0.4191 and 0.4329, respectively. The creep indexes ($C_{\alpha e}$) are 0.0097 and

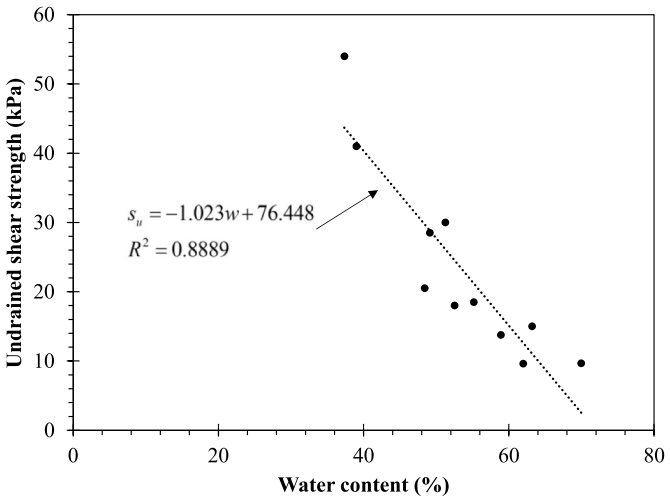

Fig. 18. Relationship between undrained shear strength and water content.

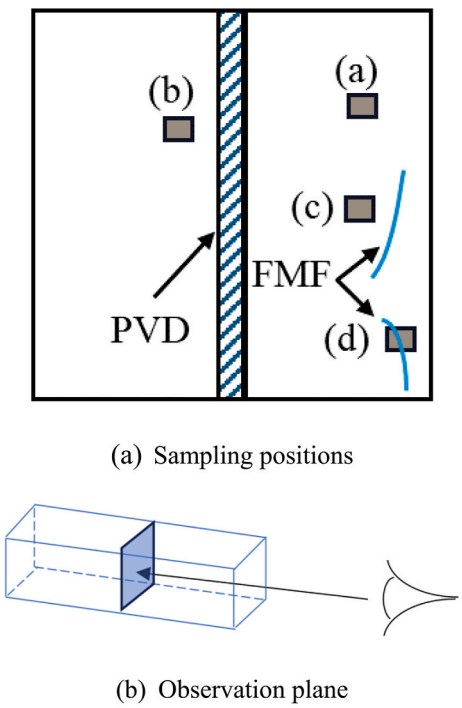

Fig. 19. Sampling for SEM observation: (a) sampling positions and (b) observation plane.

0.0100, respectively. The C_c of FMF-treated soil is slightly higher than that of pure HKMD. However, the continuous settlement in Test 3 indicates a higher consolidation efficiency instead of the higher compressibility only. The influence of compressibility on the final settlement difference is quite insignificant (i.e. around 1%). A portion of the settlement corresponding to a load of 80 kPa cannot be achieved due to the malfunction of the PVD at the later stage of the tests without FMF, whereas the FMF facilitates greater consolidation settlement, particularly after the PVD undergoes severe bending. The consolidation would cease earlier with a larger settlement if only the higher compressibility influences.

3.2. Excess porewater pressure

The porewater pressure was monitored by pressure transducers. Because the water level and soil height decreased with consolidation, the static water pressure and total water pressure varied. Therefore, excess porewater pressure is employed in this section to reflect the effect of vacuum load. The water level was monitored during tests so that the static water pressure could be calculated. Then the effective stress principle is used to derive the excess porewater pressure. Fig. 12 plots the excess porewater pressure of three tests.

Fig. 12a shows that the vacuum pressure from the pump was relatively stable and maintained at −80 kPa since Day 6 as the pump setting in Test 1. The pressure at $h = 25$ cm reached its stable state on Day 12, while the pressures at $h = 15$ cm and $h = 5$ cm successively became steady a few days later. The stable pressures at the three heights are all higher than the pump pressure. It indicates that the vacuum was lost during the transmission. The soil at $h = 25$ cm is closer to the vacuum entry, so the energy loss is relatively small with a larger negative pressure. In contrast, the soil at $h = 5$ cm is far from the vacuum source. The applied vacuum was consumed more along the path, resulting in a higher stable pressure. Slight fluctuations can be attributed to the vacuum pump and the self-adjustment of the sealing membrane during settlement. In addition, it takes more time to reach a stable state when the soil is far from the vacuum entry.

In contrast to Test 1, excess porewater pressure variations of Test 2 at different heights show similar patterns without significant differences (Fig. 12b), which means the vacuum load uniformly worked on each soil layer. The final excess porewater pressures at these positions are all around −64 kPa, which is higher than the CPVD case. This can be attributed to the dense soil layer with low permeability formed around the PVD under the vacuum pressure, called clogging zone. The clogging zone hindered the transfer of vacuum pressure. The clogging zone formed around the EPVD may be denser and have a lower permeability than the CPVD, resulting in higher pressures. The pressures within the soil were smaller than the pump pressure, indicating that vacuum loss occurred along the path due to clogging. On the other hand, the pressure distribution along the depth is relatively uniform in Test 2, indicating that the vacuum load is more effectively transferred to the whole soil layer using EPVD than CPVD. The reason can be attributed to the CPVD severely bending at the higher position, whereas the EPVD remained smooth. This will be discussed in a later section.

Like the results of Test 2, the excess porewater pressures at the three heights in Test 3 show similar responses to the applied vacuum pressure (Fig. 12c). The −60 kPa pressure was reached on Day 12, which is consistent with Test 2. However, the excess porewater pressure kept decreasing and finally reached −80 kPa on Day 17, showing almost no vacuum loss. The reason can be that the FMF provided extra channels within the soil facilitating smooth movement of both vacuum pressure and porewater. The pressure inside the model remained consistent with the pump pressure, and even a fluctuation caused by the pump was also observed. Despite the fluctuations, the average level of the internal pressure remained at approximately −74 kPa, which is still better than the other two tests.

EPVD transfer the vacuum pressure more efficiently than the CPVD, reaching a stable pressure earlier. However, the higher efficiency also induces a denser clogging zone around EPVD. This result is consistent with the study of Wang et al. (2021). Besides, vacuum loss seems unavoidable in cases without FMF due to the drain bending or clogging. The excess porewater pressure of Test 1 and Test 2 cannot meet the pump pressure, whereas Test 3 did. FMF provided extra channels for the vacuum pressure transmission and porewater dissipation in Test 3. Consequently, the vacuum load efficiently worked on the soil without loss. This explained why the soil exhibited a notably higher settlement in Test 3, particularly after the PVD malfunction.

In engineering practices, the vacuum loss is one of the major reasons that influence the effectiveness of vacuum preloading. Vacuum loads hardly reach deep areas, particularly after PVD is severely bent. The load generated by vacuum pumps cannot effectively act on the whole soil mass. The above findings from tests reveal that FMF enhances vacuum

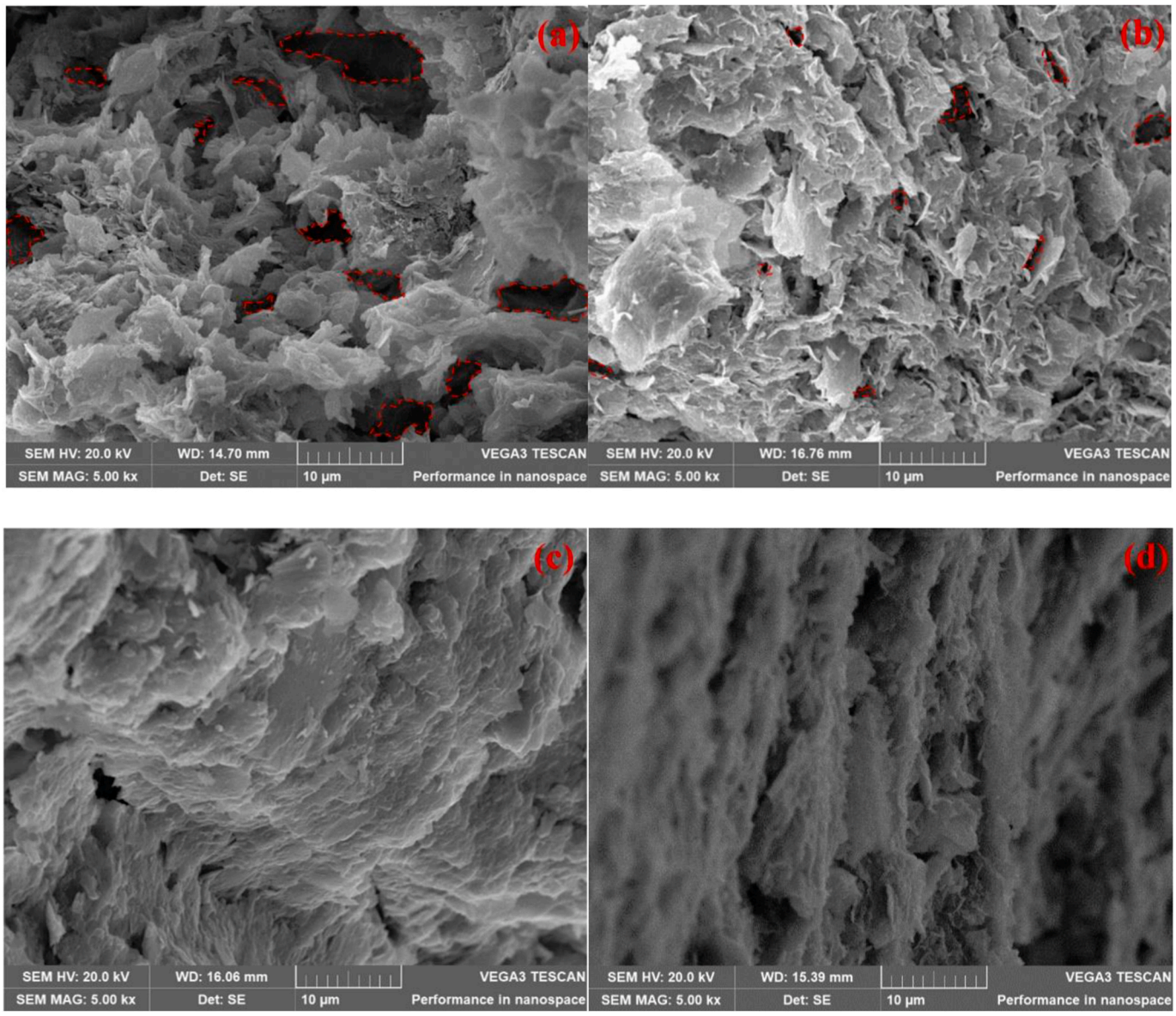

Fig. 20. SEM photos of HKMD after tests for soils (a) away from PVD in Test 2, (b) close to PVD in Test 2, (c) away from the PVD but near the FMF in Test 3, and (d) attached to FMF in Test 3.

preloading by providing additional channels so that less vacuum was wasted on the transmission path. Thus, the application of the proposed FMF-treated soil technique would considerably improve the vacuum treatment efficiency and effectiveness by minimizing vacuum loss.

Although fluctuations occurred, the general characteristics of the variation of excess porewater pressure of soils treated by different PVDs and FMF with vacuum load can be observed. Most importantly, the observed excess porewater pressure profiles along the depth show differences from each other (Fig. 13). In ideal conditions, the theoretical pressure distribution along the depth under PVD vacuum load is assumed to be a straight line.

On Day 10, the excess porewater pressure profile of Test 3 is far lower than that of Test 1 and Test 2. The FMF considerably improved the efficiency of vacuum preloading. Moreover, the curve of Test 2 is on the left to the curve of Test 1, indicating that EPVD outperformed CPVD in the early stage. On the other hand, comparing the maximum pressure distributions, the vacuum in the test using EPVD incorporated with FMF (i.e. Test 3) is uniformly distributed along the depth, which shows a similar pattern and is closest to the assumed line. However, tests without FMF cannot make it.

3.3. Water content

Soil samples were taken from the model inside through sampling ports at different times and different heights during the whole test period. The variation of the average water content of the entire soil layer thus can be determined based on the vertical distribution of water content. Though the heterogeneity of HKMD and the measuring accuracy attributed to the difference in the water content at the initial stage among the three tests, the influence of vacuum preloading on the water content variation can still be observed.

Fig. 14 shows that vacuum load accelerated the consolidation among all tests. Tests using EPVDs (i.e. Test 2 and Test 3) consolidated faster at the early stage. The average water content dropped to approximately 60% on Day 10. Then the consolidation in Test 2 slowed down and the curve became almost flat. The consolidation rate of the case using CPVD (i.e. Test 1) was slower than the EPVD case, but its significant consolidation continued until Day 18. Then the average water content basically

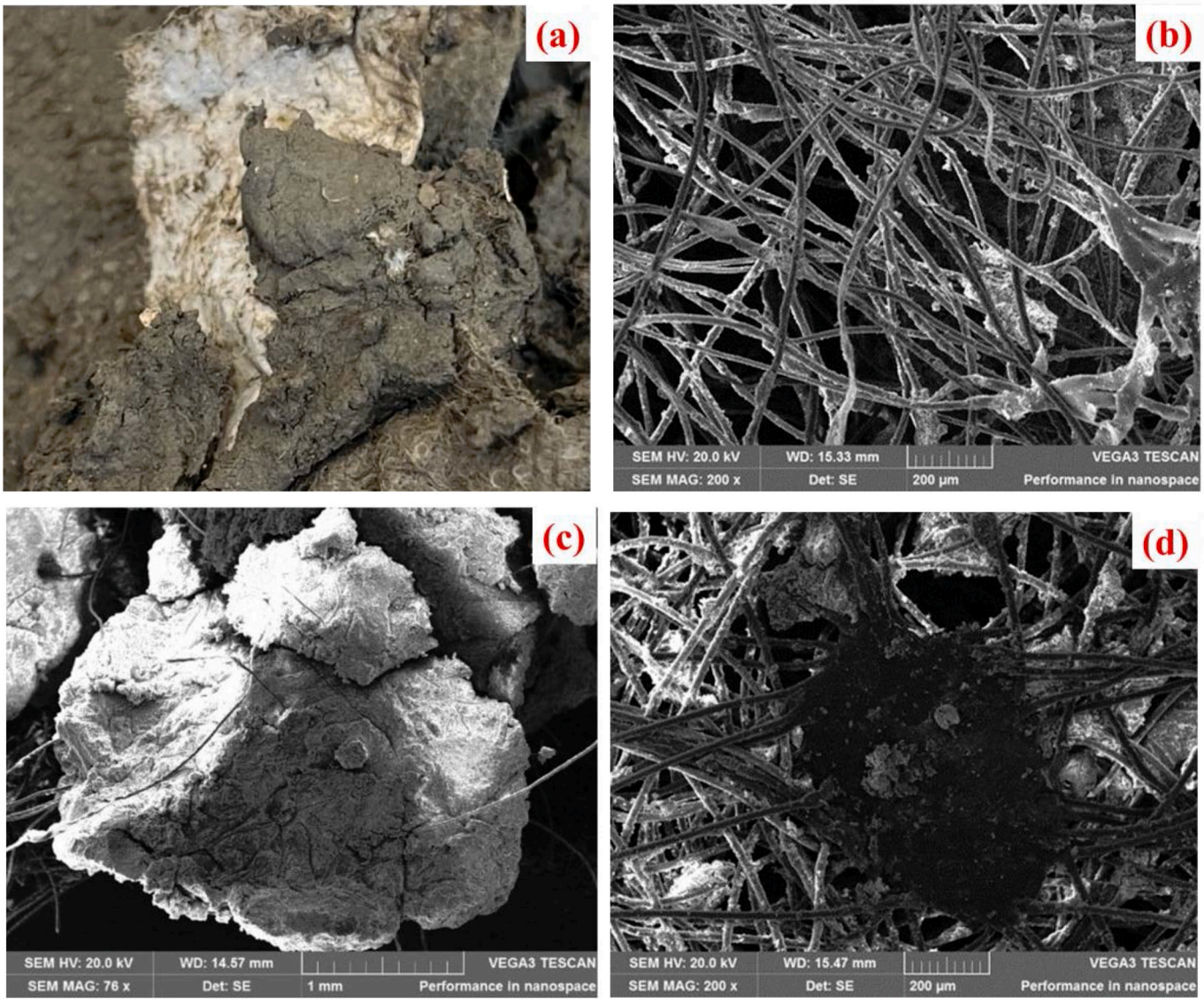

Fig. 21. FMF in treated soils: (a) FM piece, (b) FM piece under SEM, (c) a soil floc with FM fibre core, and (d) soils tightly attached to FM fibre.

remained unchanged. Meanwhile, face mask fibres induced a considerable decrease in the average water content after the PVD ceased working in Test 3. Though there seems no change in water content in Test 2 after Day 10, the value kept decreasing in Test 3. The final average water contents of Test 1, Test 2 and Test 3 are 65.48%, 57.50% and 41.82%, respectively. Due to the slight difference in average water content before vacuum loading among the three tests, the final percentage reductions of average water content (R_w), which is defined in a similar way to the final strain, are calculated using the following equation for convenient comparison.

$$R_w = \frac{w_1 - w_f}{w_1} \tag{3}$$

Results are listed in Table 5. Both the absolute decrease and the relative decrease in average water content indicate that the FMF reduced the water content the most. Particularly, the final average water content of the test with FMF is considerably lower than the liquid limit.

As shown in Fig. 15, the final water content gradually increases along the depth for all tests, consistent with the boundary conditions. The soil surface is the top drainage boundary that is closest to the vacuum source, so the water here could be first drained. The final average water contents of Test 1 and Test 2 are close to the liquid limit of HKMD, indicating that the soils remain excessively soft, particularly the lower parts that retain a liquid-like state. The FMF-treated soil reached a better result as the final water content of the whole soil layer was far lower than the liquid limit. This is a significant improvement compared to the conventional vacuum preloading treatment without adding FMF.

Soils were also sampled at different radial distances to the model centre at test ends to investigate the radial water content distribution. The distributions of final water content in the radial direction of the top and bottom layers are shown in Fig. 16. It clearly shows an increasing trend from centre to sidewall in the top layers of Test 1. The reason is that the centre soil is closest to the drainage boundary, so the water content decreased faster. However, the topsoil of Test 2 and Test 3 show no significant difference in the radial profile, which is consistent with the excess porewater pressure distribution. The clogging zone with lower permeability quickly formed around the EPVD due to its higher drainage efficiency. The dissipation of porewater is controlled and limited earlier by the clogging zone in the radial direction. Vertical drainage becomes a major way for porewater dissipation at the top layer because it is close to the top drainage boundary. Therefore, the difference in water content in the radial direction is not apparent.

Regarding the bottom soil layers, Test 1 and Test 3 show no clear trend in the radial direction. But a slight increase trend could be seen in

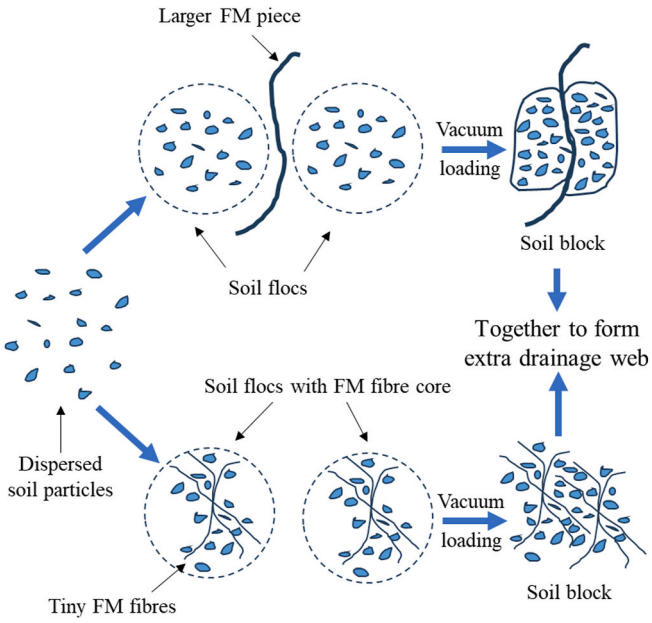

Fig. 22. Schematic of the FMF improvement mechanisms.

Test 2. PVD bending could be the reason. Sharp bends existed at higher positions in Test 1 and Test 3, while there were several smooth arcs in Test 2 PVD. The drainage and vacuum transmission could be severely blocked at the sharp bends. The lower part of a PVD would thus malfunction. The porewater of lower soils can only be dissipated vertically through the soil structure, especially in Test 1. On the other hand, the FMF uniformly assisted the drainage within the whole soil in Test 3. Therefore, the radial trend could not be formed under these conditions. Nevertheless, the smooth bends exhibit slight influences on the PVD drainage efficiency in Test 2.

3.4. Undrained shear strength

Undrained shear strength is another important parameter to judge the quality of soil improvement. In this study, the vane shear test was employed to determine the undrained shear strength of soils treated by vacuum preloading, and the results are compared in Fig. 17.

Two or three points were measured at each height and marked by hollow marks. Solid marks and lines indicate the average profile. It shows that the vane shear strengths of the soils after Test 1 and Test 2 are very close to each other, which is consistent with the settlement and water content. The average strengths in Test 1 and Test 2 increase from 9.6 kPa at the bottom (i.e. 5 cm) to around 18 kPa at $h = 25$ cm. Because the soil surfaces inclined during tests, the strengths of the top layers were measured at different heights. In Test 2, the shear strength profile is a straight line along the depth. The top strength is 20.5 kPa in Test 2, whereas it rapidly increases to 30 kPa at the top in Test 1 due to the measuring point being very close to the PVD connector. The ventilation is significant, resulting in a stiff crust here. In general, the vane shear strength shows a linear increase from the bottom to the top and the two types of PVD performed similarly. Compared to the other two tests, the undrained shear strength of the FMF-treated soil is greatly improved. In Test 3, the lowest strength of 28.5 kPa occurred at the bottom, and the highest occurred at the top with 54 kPa.

On the other hand, the undrained shear strength is related to water content. Recent studies (Wahls, 1983; Zhang et al., 2021a, 2021b) reveal that the relationship between undrained shear strength and water content for a certain soil shows an approximate linear pattern. This conclusion is consistent with the results from the present study (Fig. 18). With the decrease in water content, the corresponding undrained shear strength increases. The proposed FMF-treated soil technique considerably enhances the efficiency of vacuum consolidation, thereby higher shear strength could be attained with the lower water content. In addition, the FMF also serves as a reinforcement material in the soil. Previous studies using other plastic fibres have explored the impact of fibre reinforcement on soil strength (Tang et al., 2010, 2016). Their findings indicate a significant increase in soil peak strength with fibre inclusion. The vane shear test conducted in this study validates this conclusion.

3.5. Microstructure analysis

Microstructure determines soil behaviour. Scanning electron microscope is a widely used technique to study microstructures, and it was employed in this research. Soil samples at different positions (Fig. 19a) were freeze-dried for SEM analysis. The soil samples were first cut into small cuboids from the column. The long edge of the cuboid is perpendicular to the direction of gravity. After freeze-drying, the samples were manually broken at the centre to expose the observation plane as Fig. 19b shows.

Comparing the micrographs of Fig. 19a and b, particles of soils away from and near the PVD show relatively random arrangement. However, the micrograph of the soil away from PVD exhibits more and larger pores, while the soil near PVD seems relatively denser. However, apparent pores remained in soils without FMF. On the other hand, the SEM photos of Test 3 (Fig. 20c and d) show that the layered structure was formed near FMF. Soil particles lay layer by layer. Especially, a dense layered structure like book pages was observed in the soil attached to the FMF (Fig. 20d). The microstructure influences the mechanical properties such as the shear strength. Soils are bonded more tightly in the dense structure, resulting in a higher shear strength. The SEM observation is consistent with the undrained shear strength results. For instance, the shear strength near the PVD is higher than that away from PVD.

Before freeze-drying these specimens, water contents were determined using surrounding soils. The water contents of soils corresponding to Fig. 20a and (b) (c) and (d) are 61.72%, 52.68%, 38.93% and 35.64%, respectively. It can be found that the layered structure can be formed if the water content is notably lower than the liquid limit (i.e. $w_L = 64\%$). Although the water contents of the SEM samples of Fig. 20a and (b) are slightly lower than the liquid limit, the stable layered microstructure is not formed and large pores can be observed in the electron micrograph. The vacuum pressure and porewater thus can easily move through these large pores. Therefore, the vacuum loss may happen less when it passes these pores, and the consolidation is faster as a result. However, when the vacuum pressure attempted to cross the dense zone surrounding the PVD, the efficiency significantly dropped if no FMF was added. The larger pores lead to a higher permeability, while the dense microstructure exhibits a lower permeability. However, FMF-treated soil simultaneously exhibits a denser microstructure and ongoing settlement. Although the paths in the soil were narrowed or blocked, the FMF provide extra channels for vacuum transfer and drainage. The microstructure indicates the significant impact of FMF on permeability.

Two mechanisms of how FMF works are noticed from the microscopic observation. First, the larger face mask piece works as a single drainage channel. This kind of FMF remained clean during the test, as shown in Fig. 21a and (b) on both macro and micro scales. It indicates that no soil particles clog the drainage channel and the vacuum pressure as well as porewater can smoothly move along this path. Numerous channels form a web to transfer the vacuum pressure and porewater so that the vacuum load can quickly work on the whole soil layer. In the second mode, soil particles were first attracted around tiny face mask fibres to form larger soil flocs, and the fibres served as the floc cores (Fig. 21c). Soil particles were gradually adsorbed to the core during the sedimentation and self-weight consolidation. Each soil floc further contracted toward its fibre core under the vacuum load. In this mode, soil particles are tightly attached to the face mask fibres as shown in

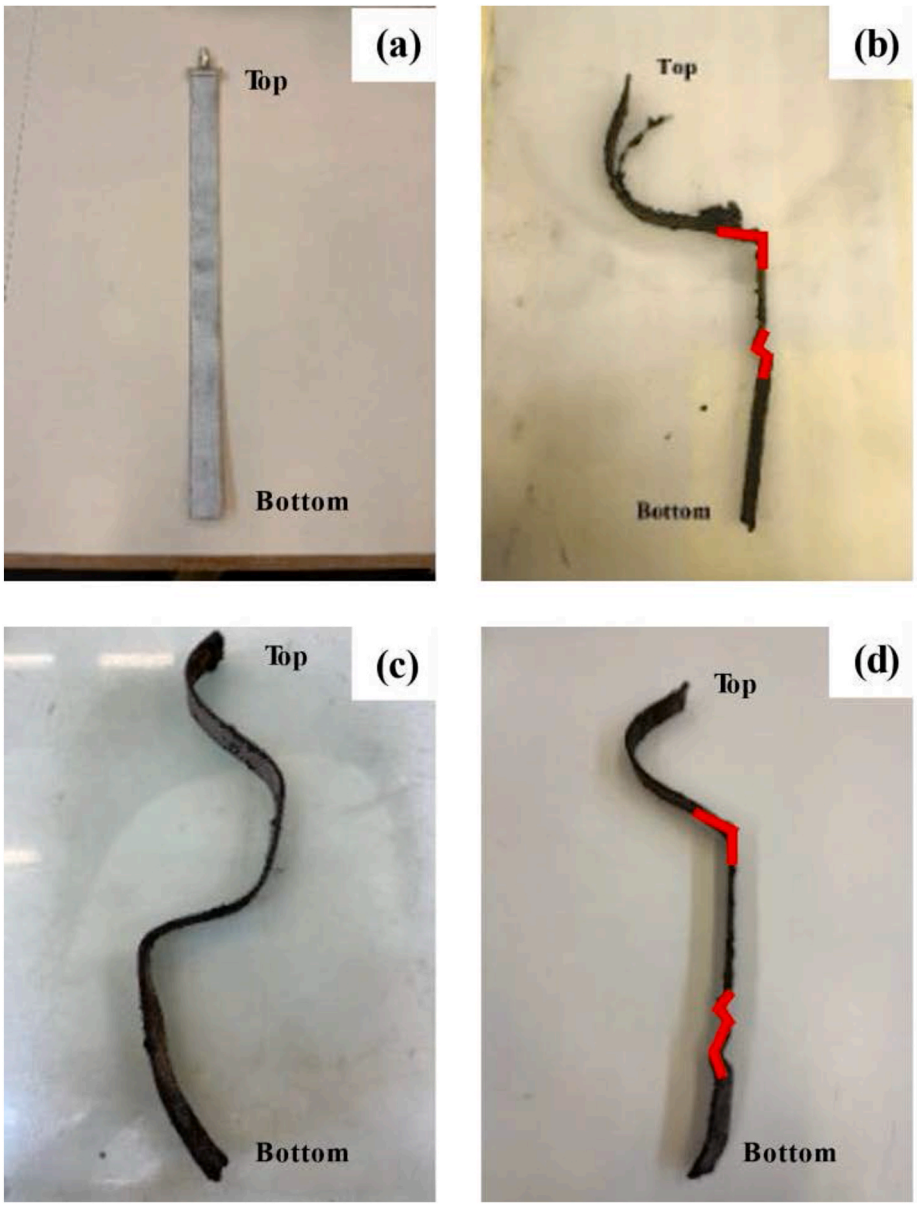

Fig. 23. Photos of PVD: (a) before installation, (b) after Test 1, (c) after Test 2, and (d) after Test 3.

Fig. 21d. Another drainage web was formed among these individual soil flocs. The two mechanisms work together to develop a large drainage web to improve vacuum preloading efficiency, as illustrated in Fig. 22. This is consistent with the result of excess porewater pressure, as the pressure inside the soil of Test 3 could reach the lowest value and match the pressure generated by the vacuum pump.

On the other hand, the FMF could also serve as a reinforcement material to enhance the strength of the treated soil. The reduced water content could contribute to this enhanced strength, while the bonding effect of FMF stands out as another primary factor. SEM photos clearly show soil particles tightly adhering to the fibres, thereby resulting in an increasing shear resistance.

To sum up, the FMF greatly alters the microstructure of soil, which in turn affects both vacuum consolidation and strength.

3.6. PVD after test

After the tests, PVDs used in Test 1, Test 2 and Test 3 were taken out for observation (Fig. 23). It clearly shows that all three PVDs bent a lot during the test. However, the PVDs exhibited various bending patterns among the three tests. The Test 1 PVD deformed severely with a 90-degree bending. The vacuum load may be significantly blocked at this position, resulting in higher pressure at the lower part. The Test 2 PVD shows several smooth arcs from the top to the middle position but is not as severe as Test 1. The Test 3 PVD was mainly bent at the upper part, and small wrinkles occurred at the lower part. Generally, two types of bending were observed: smooth arcs and sharp bends. The sharp bends would severely reduce the PVD drainage efficiency, while the smooth arcs would have less influence. The sharp bends are marked with red lines in Fig. 23. A sharp bend resembles a fracture, causing the internal drainage channel to break. Consequently, the vacuum load cannot be effectively transmitted through it, impeding the upward movement of pore water through these channels. These sharp bends could be the reason why the settlement rate decreased significantly a few days after the CPVD installations in Test 1, whereas the slowdown in settlement is mainly due to the clogging around the EPVD in Test 2. After that, the movement of porewater via the PVD slows down. The drainage web formed by FMF became the primary way to dissipate the porewater in Test 3. Therefore, the consolidation seems to have ceased in Test 1 and Test 2, while the soil kept settling in Test 3. The results obtained from

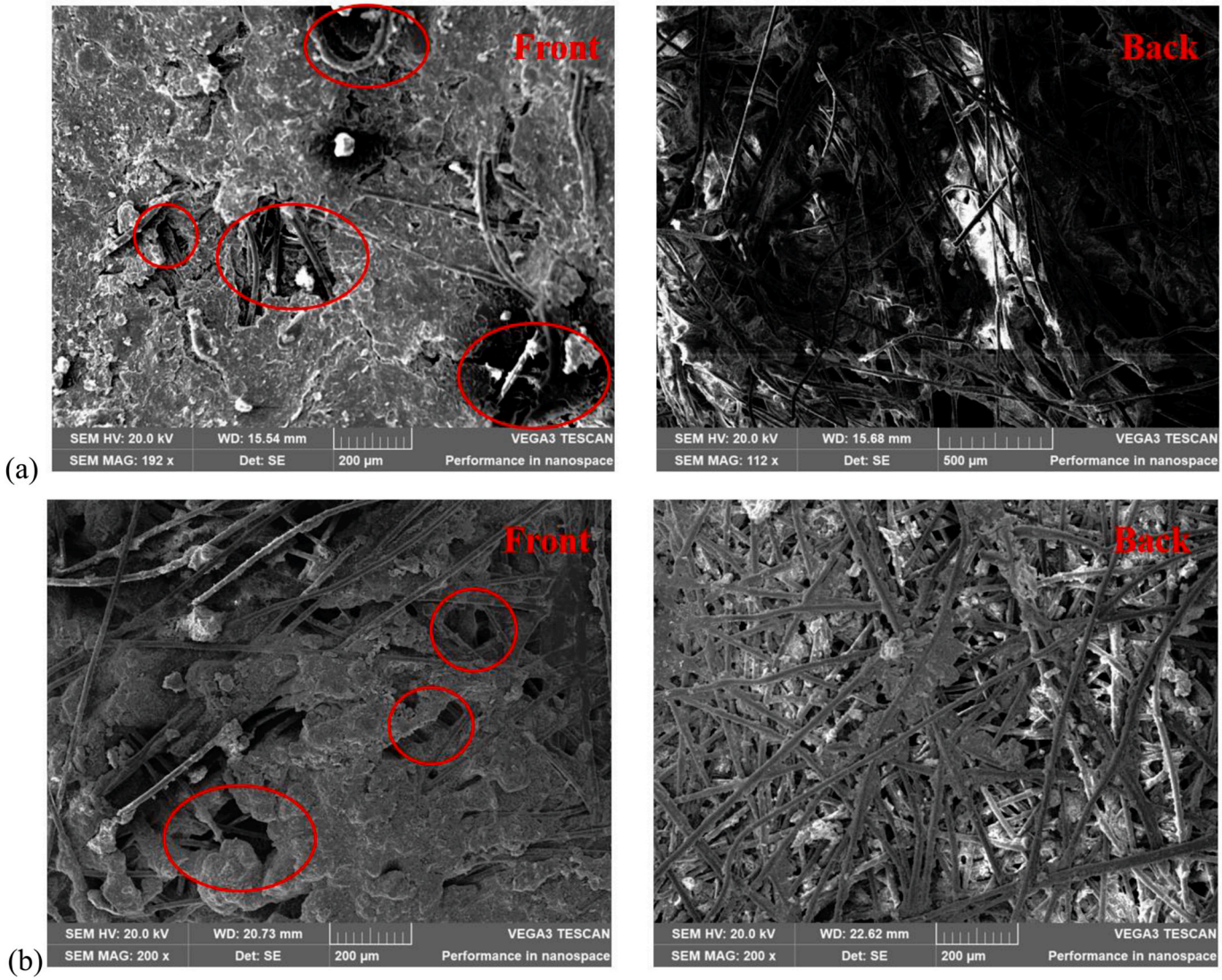

Fig. 24. SEM photos of PVD after vacuum consolidation tests: (a) CPVD filter after Test 1, and (b) EPVD filter after Test 2.

this research are consistent with previous studies conducted by other researchers (Cai et al., 2017).

Furthermore, the filters of PVDs used in Test 1 and Test 2 were peeled off for microscopic observation (Fig. 24). Micrographs show that most front areas of both PVD filters are covered by soil particles, and few open channels exist (i.e. the circled area). The clogging will considerably reduce the drainage efficiency of PVD itself and affect the consolidation rate. Thus the test results could be influenced. However, the range of clogging zone is limited. The soil of the SEM photo Fig. 20a lies only a few centimetres away from the PVD, but the large pores still exist. On the back side of the PVD filter, it can be seen that soil particles were blocked outside. The internal channels of PVDs remained clean.

4. Conclusions

This study proposed a method of face mask fibres combined with PVD and vacuum preloading for soft soil improvement. The effectiveness of this method was examined by conducting a series of laboratory tests. The major conclusions drawn from this study are as follows.

(1) The face-mask fibre significantly improves the treatment effects and efficiency of vacuum preloading. More vacuum pressure was transmitted to the soil with the use of FMF. The soil thickness and water content kept decreasing even after 30 days using the new method. The final water content of the FMF-treated soils is considerably lower than the liquid limit. Traditional vacuum preloading cannot yield such value.

(2) Face-mask fibre works with two mechanisms to improve the efficiency of vacuum preloading. The first mode is that the large face mask piece works as a single drainage channel. Soil flocs are attracted to the larger FMF and consolidate under vacuum load. The second is tiny face-mask fibres serving as the core of soil floc. Soil particles are firstly adsorbed to the fibre to form a soil-fibre floc. Individual flocs then consolidated toward their own fibre cores under vacuum load. The two mechanisms work together to develop a drainage web in the soil. After the PVD malfunctions, the web formed by FMF plays a key role in soil consolidation.

(3) The characteristics of the two types of PVD vary during the tests. The CPVD is severely bent during vacuum consolidation, while the EPVD bends with several smooth curves so that the EPVD's workability along the depth is less affected. On the other hand, the clogging zone formed around the EPVD is denser than that of the CPVD due to the higher efficiency of EPVD.

(4) The proposed method utilizes waste face masks and eco-friendly PVDs made from crop stalks, an agricultural waste, alleviating the burden on waste management and promoting environmental

benefits. The utilization of both materials leads to savings in both waste management and construction material costs, contributing to sustainable geotechnical practices. Additionally, this approach not only addresses waste management challenges but also enhances the efficiency and effectiveness of vacuum preloading, resulting in reduced electricity costs.

Given the uncertainties accompanying real construction conditions, conducting a field trial test would be a preferable method to investigate the proposed FMF-treated soil technique in the future, particularly exploring the long-term degradation of FMF and EPVD. Furthermore, all products manufactured using nonwoven fabric can potentially serve as admixtures for soil improvement. It is interesting to identify the optimal type of waste fibres from various sources for soil improvement in future research.

CRediT authorship contribution statement

Kai Lou: Writing – original draft, Validation, Methodology, Investigation, Formal analysis, Data curation. **Zhen-Yu Yin:** Writing – review & editing, Supervision, Resources, Project administration, Methodology, Funding acquisition, Formal analysis, Conceptualization. **Ding-Bao Song:** Writing – review & editing, Methodology, Investigation. **Wei-Feng Huang:** Writing – review & editing, Validation, Investigation, Data curation.

Declaration of competing interest

The authors declare that they have no known competing financial interests or personal relationships that could have appeared to influence the work reported in this paper.

Acknowledgements

The work in this paper is supported by a Research Impact Fund (RIF) project (R5037-18), a General Research Fund (GRF) projects (15217220) and a NSFC/RGC Joint Research Scheme (N_PolyU534/20) from Research Grants Council (RGC) of Hong Kong Special Administrative Region Government of China.

Data availability

Data will be made available on request.

References

ASTM, 2017. ASTM D2487-17e1 Standard Practice for Classification of Soils for Engineering Purposes. Unified Soil Classification System).
ASTM, 2022. ASTM D6917-16 Standard Guide for Selection of Test Methods for Prefabricated Vertical Drains (PVD).
Barforoush, A.R., Almustafa, M., Shooshpasha, I., MolaAbasi, H., Nehdi, M.L., 2024. Triaxial Drained Behaviour of Disposable Face Mask Fibre Reinforced Sand. Geomechanics and Geoengineering 1–17.
Bergado, D.T., Saowapakpiboon, J., Kovittayanon, N., Zwart, T., 2008. BeauDrain-S PVD vacuum system in soft bangkok clay : a case study of the suvarnabhumi airport project. In: The 6th Sysposium on Soft Ground Improvement and Geosythetics, vol. 10.
British Standards Institution, 2016. BS1377:2016 Methods of Test for Soils for Civil Engineering Purposes. British Standards Institution, London.
Cai, Y., Qiao, H., Wang, J., Geng, X., Wang, P., Cai, Y., 2017. Experimental tests on effect of deformed prefabricated vertical drains in dredged soil on consolidation via vacuum preloading. Eng. Geol. 10–19.
Chai, J.-C., Carter, J.P., Hayashi, S., 2006. Vacuum consolidation and its combination with embankment loading. Can. Geotech. J. 43, 985–996.
Chai, J.-C., Hong, Z., Shen, S., 2010. Vacuum-drain consolidation induced pressure distribution and ground deformation. Geotext. Geomembranes 28, 525–535.
Chai, J.C., Carter, J.P., 2013. Consolidation theory for combined vacuum pressure and surcharge loading. 18th International Conference on Soil Mechanics and Geotechnical Engineering, pp. 2449–2452. Paris.
Chu, J., Bo, M.W., Arulrajah, A., 2009. Reclamation of a slurry pond in Singapore. Proceedings of the Institution of Civil Engineers - Geotechnical Engineering 162, 13–20.
Chu, J., Yan, S., Lam, K.P., 2012. Methods for improvement of clay slurry or sewage sludge. Proc. Inst. Civ. Eng.: Ground Improv. 165, 187–199.
Corlever, N.G., Visser, G.T., De Zwart, T.P., 2006. PVD Ground improvement with vacuum preloading at Suvarnabhumi Airport. In: Bergado, D.T. (Ed.), Proceedings of the International Symposium on Geotechnical Aspects of Suvarnabhumi Airport in Thailand. Southeast Asian Geotechnical Society (SEAGS). Bangkok, Thailand.
Dong, P.H., 2018. Influence of vertical drains on improving dredged mud by vacuum consolidation method. Journal of Science and Technology in Civil Engineering (STCE) - NUCE 12, 63–72.
Fang, Z., Yin, J.-H., 2006. Physical modelling of consolidation of Hong Kong marine clay with prefabricated vertical drains. Can. Geotech. J. 43, 638–652.
Hansbo, S., 1960. Consolidation of Clay, with Special Reference to Influence of Vertical Sand Drains, vol. 160. Proceeding of Royal Swedish Geotechnical Institute.
Hansbo, S., 1979. Consolidation of clay by band-shaped prefabricated drains. Ground Eng. 12, 16–25.
Hansbo, S., Jamiolkowski, M., Kok, L., 1981. Consolidation by vertical drains. Geotechnique 31, 45–66.
Jeon, H.Y., Kim, S.H., Chung, Y.I., Yoo, H.K., Mlynarek, J., 2003. Assessments of long-term filtration performance of degradable prefabricated geotextile drains. Polym. Test. 22, 779–784.
Jewell, R.A., 1996. Soil Reinforcement with Geotextiles. Thomas Telford, Westminster.
Kaewthai, N., Chooglin, S., 2015. Physical and Mechanical Properties of Corn Stalk for Being Used as Raw Material for Prefacbricated Vertical Drain.
Kilmartin-Lynch, S., Saberian, M., Li, J., Roychand, R., Zhang, G., 2021. Preliminary evaluation of the feasibility of using polypropylene fibres from COVID-19 single-use face masks to improve the mechanical properties of concrete. J. Clean. Prod. 296, 126460.
Kjellman, W., 1948. Accelerating consolidation of fine grain soils by means of cardboard wicks. Proc. 2nd ICSMFE 2, 302–305. Rotterdam, 1948.
Kumarage, P.I., Gnanendran, C.T., 2019. Long-term performance predictions in ground improvements with vacuum assisted Prefabricated Vertical Drains. Geotext. Geomembranes 47, 95–103.
Lam, K.P., Wu, S., Chu, J., 2020. Field trial of a membraneless vacuum preloading system for soft soil improvement. Proceedings of the Institution of Civil Engineers - Ground Improvement 173, 40–50.
Lee, S.L., Karunaratne, G.P., Ramaswamy, S.D., Aziz, M.A., Das Gupta, N.C., 1994. Natural geosynthetic drain for soil improvement. Geotext. Geomembranes 13, 457–474.
Liu, H.-l., Chu, J., 2009. A new type of prefabricated vertical drain with improved properties. Geotext. Geomembranes 27, 152–155.
Long, P.V., Nguyen, L.V., Bergado, D.T., Balasubramaniam, A.S., 2015. Performance of PVD improved soft ground using vacuum consolidation methods with and without airtight membrane. Geotext. Geomembranes 43, 473–483.
Ngo, D.H., Horpibulsuk, S., Suddeepong, A., Hoy, M., Udomchai, A., Doncommul, P., Rachan, R., Arulrajah, A., 2020. Consolidation behavior of dredged ultra-soft soil improved with prefabricated vertical drain at the Mae Moh mine, Thailand. Geotext. Geomembranes 48, 561–571.
Nguyen, H.-S., Tashiro, M., Inagaki, M., Yamada, S., Noda, T., 2015. Simulation and evaluation of improvement effects by vertical drains/vacuum consolidation on peat ground under embankment loading based on a macro-element method with water absorption and discharge functions. Soils Found. 55, 1044–1057.
Nguyen, T., Indraratna, B., Baral, P., 2020. Biodegradable prefabricated vertical drains: from laboratory to field studies. Geotech. Eng. 51, 39–46.
Nguyen, T.T., Indraratna, B., 2017a. Experimental and numerical investigations into hydraulic behaviour of coir fibre drain. Can. Geotech. J. 54, 75–87.
Nguyen, T.T., Indraratna, B., 2017b. The permeability of natural fibre drains, capturing their micro-features. Proceedings of the Institution of Civil Engineers - Ground Improvement 170, 123–136.
Nguyen, T.T., Indraratna, B., 2023. Natural fibre for geotechnical applications: concepts, achievements and challenges. Sustainability 15, 8603.
Nguyen, T.T., Indraratna, B., Carter, J., 2018. Laboratory investigation into biodegradation of jute drains with implications for field behavior. J. Geotech. Geoenviron. Eng. 144, 04018026.
Rehman, Z.U., Khalid, U., 2021. Reuse of COVID-19 face mask for the amelioration of mechanical properties of fat clay: a novel solution to an emerging waste problem. Sci. Total Environ. 794, 148746.
Saberian, M., Li, J., Kilmartin-Lynch, S., Boroujeni, M., 2021. Repurposing of COVID-19 single-use face masks for pavements base/subbase. Sci. Total Environ. 769, 145527.
Tang, C.-S., Paleologos, E.K., Vitone, C., Du, Y.-J., Li, J.-S., Jiang, N.-J., Deng, Y.-F., Chu, J., Shen, Z., Koda, E., Dominijanni, A., Fei, X., Vaverková, M.D., Osiński, P., Chen, X., Asadi, A., Takeuchi, M.R.H., Bo, M.W., Abuel-Naga, H., Leong, E.-C., Farid, A., Baser, T., O'Kelly, B.C., Jha, B., Goli, V.S.N.S., Singh, D.N., 2021. Environmental geotechnics: challenges and opportunities in the post-Covid-19 world. Environmental Geotechnics 8, 172–192.
Tang, C.-S., Shi, B., Zhao, L.-Z., 2010. Interfacial shear strength of fiber reinforced soil. Geotext. Geomembranes 28, 54–62.
Tang, C.-S., Wang, D.-Y., Cui, Y.-J., Shi, B., Li, J., 2016. Tensile strength of fiber-reinforced soil. J. Mater. Civ. Eng. 28, 04016031.
Wahls, H.E., 1983. Undrained shear strength of saturated clay. Transport. Res. Rec.
Wang, J., Cai, Y., Fu, H., Hu, X., Cai, Y., Lin, H., Zheng, W., 2018. Experimental study on a dredged fill ground improved by a two-stage vacuum preloading method. Soils Found. 58, 766–775.
Wang, J., Cai, Y., Liu, F.Y., Li, Z., Yuan, G.H., Du, Y.G., Hu, X.Q., 2021. Effect of a vacuum gradient on the consolidation of dredged slurry by vacuum preloading. Can. Geotech. J. 58, 1036–1044.

Wang, J., Cai, Y., Ma, J., Chu, J., Fu, H., Wang, P., Jin, Y., 2016. Improved vacuum preloading method for consolidation of dredged clay-slurry fill. J. Geotech. Geoenviron. Eng. 142, 06016012.
Wang, L., Li, S., Ahmad, I.M., Zhang, G., Sun, Y., Wang, Y., Sun, C., Jiang, C., Cui, P., Li, D., 2023a. Global face mask pollution: threats to the environment and wildlife, and potential solutions. Sci. Total Environ. 887, 164055.
Wang, Z., Zhang, W., Wei, M., Wang, P., Li, D., 2023b. Mechanical and deformation behavior of clay reinforced by discarded mask fibers. J. Clean. Prod. 428, 139485.
Wu, Y., Zhou, R., Lu, Y., Zhang, X., Zhang, H., Tran, Q.C., 2022. Experimental study of PVD-improved dredged soil with vacuum preloading and air pressure. Geotext. Geomembranes 50, 668–676.
Yuan, W., Deng, Y., Ying, Z., Yang, Q., Su, Y., Hong, Z., 2024. Degradation of straw-based wick drain and its effect on consolidation. J. Clean. Prod. 452, 142182.
Zhang, P., Jin, Y.-F., Yin, Z.-Y., 2021a. Machine learning–based uncertainty modelling of mechanical properties of soft clays relating to time-dependent behavior and its application. Int. J. Numer. Anal. Methods GeoMech. 45, 1588–1602.
Zhang, P., Yin, Z.-Y., Jin, Y.-F., 2021b. Bayesian neural network-based uncertainty modelling: application to soil compressibility and undrained shear strength prediction. Can. Geotech. J. 59, 546–557.
Zhou, Y., Chen, S., Guo, W., Ren, Y., Xu, G., 2022. Recent developments in the vacuum preloading technique in China. Sustainability 14, 13897.